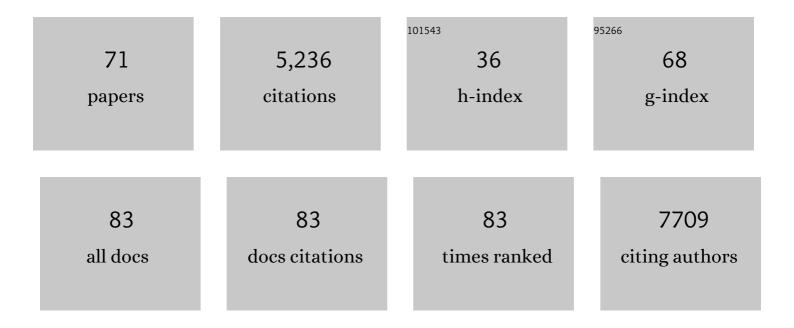
## David Izquierdo-Garcia

List of Publications by Year in descending order

Source: https://exaly.com/author-pdf/7546400/publications.pdf Version: 2024-02-01



#	Article	IF	CITATIONS
1	MRI-Based Attenuation Correction for Hybrid PET/MRI Systems: A 4-Class Tissue Segmentation Technique Using a Combined Ultrashort-Echo-Time/Dixon MRI Sequence. Journal of Nuclear Medicine, 2012, 53, 796-804.	5.0	406
2	What the left and right anterior fusiform gyri tell us about semantic memory. Brain, 2010, 133, 3256-3268.	7.6	377
3	Evidence for brain glial activation in chronic pain patients. Brain, 2015, 138, 604-615.	7.6	372
4	Design and performance evaluation of a whole-body Ingenuity TF PET–MRI system. Physics in Medicine and Biology, 2011, 56, 3091-3106.	3.0	370
5	A statin-loaded reconstituted high-density lipoprotein nanoparticle inhibits atherosclerotic plaque inflammation. Nature Communications, 2014, 5, 3065.	12.8	336
6	Different partial volume correction methods lead to different conclusions: An 18F-FDG-PET study of aging. NeuroImage, 2016, 132, 334-343.	4.2	216
7	Dopamine Release in Dissociable Striatal Subregions Predicts the Different Effects of Oral Methylphenidate on Reversal Learning and Spatial Working Memory. Journal of Neuroscience, 2009, 29, 4690-4696.	3.6	210
8	A multi-centre evaluation of eleven clinically feasible brain PET/MRI attenuation correction techniques using a large cohort of patients. NeuroImage, 2017, 147, 346-359.	4.2	200
9	Increased in vivo glial activation in patients with amyotrophic lateral sclerosis: Assessed with [11C]-PBR28. NeuroImage: Clinical, 2015, 7, 409-414.	2.7	176
10	An SPM8-Based Approach for Attenuation Correction Combining Segmentation and Nonrigid Template Formation: Application to Simultaneous PET/MR Brain Imaging. Journal of Nuclear Medicine, 2014, 55, 1825-1830.	5.0	171
11	Comparison of Methods for Magnetic Resonance-Guided [18-F]Fluorodeoxyglucose Positron Emission Tomography in Human Carotid Arteries. Stroke, 2009, 40, 86-93.	2.0	154
12	Neuroinflammatory component of gray matter pathology in multiple sclerosis. Annals of Neurology, 2016, 80, 776-790.	5.3	150
13	Disruption of thalamic functional connectivity is a neural correlate of dexmedetomidine-induced unconsciousness. ELife, 2014, 3, e04499.	6.0	135
14	Dixon-VIBE Deep Learning (DIVIDE) Pseudo-CT Synthesis for Pelvis PET/MR Attenuation Correction. Journal of Nuclear Medicine, 2019, 60, 429-435.	5.0	103
15	A positron emission tomography study of nigro-striatal dopaminergic mechanisms underlying attention: implications for ADHD and its treatment. Brain, 2013, 136, 3252-3270.	7.6	90
16	Noninvasive Assessment of Hypoxia in Rabbit Advanced Atherosclerosis Using <sup>18</sup> F-fluoromisonidazole Positron Emission Tomographic Imaging. Circulation: Cardiovascular Imaging, 2014, 7, 312-320.	2.6	90
17	Evaluation of translocator protein quantification as a tool for characterising macrophage burden in human carotid atherosclerosis. Atherosclerosis, 2010, 210, 388-391.	0.8	83
18	Glial activation colocalizes with structural abnormalities in amyotrophic lateral sclerosis. Neurology, 2016, 87, 2554-2561.	1.1	83

#	Article	IF	CITATIONS
19	MRI-based motion correction of thoracic PET: initial comparison of acquisition protocols and correction strategies suitable for simultaneous PET/MRI systems. European Radiology, 2012, 22, 439-446.	4.5	82
20	Carotid Plaque Inflammation Is Associated With Cerebral Microembolism in Patients With Recent Transient Ischemic Attack or Stroke. Circulation: Cardiovascular Imaging, 2010, 3, 536-541.	2.6	79
21	Integrated magnetic resonance imaging and [ <sup>11</sup> C]â€PBR28 positron emission tomographic imaging in amyotrophic lateral sclerosis. Annals of Neurology, 2018, 83, 1186-1197.	5.3	75
22	Deep Convolution Neural Network (DCNN) Multiplane Approach to Synthetic CT Generation From MR images—Application in Brain ProtonÂTherapy. International Journal of Radiation Oncology Biology Physics, 2019, 105, 495-503.	0.8	71
23	Simultaneous PET–MRI in oncology: a solution looking for a problem?. Magnetic Resonance Imaging, 2012, 30, 1342-1356.	1.8	66
24	Neuroinflammation in Huntington's Disease: New Insights with <sup>11</sup> C-PBR28 PET/MRI. ACS Chemical Neuroscience, 2018, 9, 2563-2571.	3.5	60
25	Watershed Infarcts in Transient Ischemic Attack/Minor Stroke With ≥50% Carotid Stenosis. Stroke, 2010, 41, 1410-1416.	2.0	57
26	The complementary roles of dynamic contrast-enhanced MRI and 18F-fluorodeoxyglucose PET/CT for imaging of carotid atherosclerosis. European Journal of Nuclear Medicine and Molecular Imaging, 2013, 40, 1884-1893.	6.4	57
27	FDC–PET can distinguish inflamed from non-inflamed plaque in an animal model of atherosclerosis. International Journal of Cardiovascular Imaging, 2010, 26, 41-48.	1.5	49
28	The relationship of topographical memory performance to regional neurodegeneration in Alzheimer's disease. Frontiers in Aging Neuroscience, 2012, 4, 17.	3.4	47
29	Arterial and fat tissue inflammation are highly correlated : a prospective 18F-FDG PET/CT study. European Journal of Nuclear Medicine and Molecular Imaging, 2014, 41, 934-945.	6.4	46
30	Improvement of Attenuation Correction in Time-of-Flight PET/MR Imaging with a Positron-Emitting Source. Journal of Nuclear Medicine, 2014, 55, 329-336.	5.0	44
31	MR Imaging–Guided Attenuation Correction of PET Data in PET/MR Imaging. PET Clinics, 2016, 11, 129-149.	3.0	43
32	Monitoring plaque inflammation in atherosclerotic rabbits with an iron oxide (P904) and 18F-FDG using a combined PET/MR scanner. Atherosclerosis, 2013, 228, 339-345.	0.8	42
33	Multisite Thrombus Imaging and Fibrin Content Estimation With a Single Whole-Body PET Scan in Rats. Arteriosclerosis, Thrombosis, and Vascular Biology, 2015, 35, 2114-2121.	2.4	42
34	Comparison of MR-based attenuation correction and CT-based attenuation correction of whole-body PET/MR imaging. European Journal of Nuclear Medicine and Molecular Imaging, 2014, 41, 1574-1584.	6.4	41
35	MRâ€assisted PET motion correction in simultaneous PET/MRI studies of dementia subjects. Journal of Magnetic Resonance Imaging, 2018, 48, 1288-1296.	3.4	41
36	Type I Collagen–targeted Positron Emission Tomography Imaging in Idiopathic Pulmonary Fibrosis: First-in-Human Studies. American Journal of Respiratory and Critical Care Medicine, 2019, 200, 258-261.	5.6	41

## DAVID IZQUIERDO-GARCIA

#	Article	IF	CITATIONS
37	[11C]PBR28 MR–PET imaging reveals lower regional brain expression of translocator protein (TSPO) in young adult males with autism spectrum disorder. Molecular Psychiatry, 2021, 26, 1659-1669.	7.9	35
38	Concurrent Respiratory Motion Correction of Abdominal PET and Dynamic Contrast-Enhanced–MRI Using a Compressed Sensing Approach. Journal of Nuclear Medicine, 2018, 59, 1474-1479.	5.0	34
39	A simultaneous [11C]raclopride positron emission tomography and functional magnetic resonance imaging investigation of striatal dopamine binding in autism. Translational Psychiatry, 2021, 11, 33.	4.8	33
40	Fungal Virulence in a Lepidopteran Model Is an Emergent Property with Deterministic Features. MBio, 2013, 4, e00100-13.	4.1	32
41	PET/MRI in the Presence of Metal Implants: Completion of the Attenuation Map from PET Emission Data. Journal of Nuclear Medicine, 2017, 58, 840-845.	5.0	32
42	Imaging Cardiovascular and Lung Macrophages With the Positron Emission Tomography Sensor <sup>64</sup> Cu-Macrin in Mice, Rabbits, and Pigs. Circulation: Cardiovascular Imaging, 2020, 13, e010586.	2.6	32
43	Preclinical Evaluation of MR Attenuation Correction Versus CT Attenuation Correction on a Sequential Whole-Body MR/PET Scanner. Investigative Radiology, 2013, 48, 313-322.	6.2	30
44	Imaging of glia activation in people with primary lateral sclerosis. NeuroImage: Clinical, 2018, 17, 347-353.	2.7	29
45	Implementation and Validation of a Three-dimensional Cardiac Motion Estimation Network. Radiology: Artificial Intelligence, 2019, 1, e180080.	5.8	29
46	Strategy for improved [11C]DAA1106 radiosynthesis and in vivo peripheral benzodiazepine receptor imaging using microPET, evaluation of [11C]DAA1106. Nuclear Medicine and Biology, 2007, 34, 439-446.	0.6	27
47	Radiation Dosimetry of the Fibrin-Binding Probe <sup>64</sup> Cu-FBP8 and Its Feasibility for PET Imaging of Deep Vein Thrombosis and Pulmonary Embolism in Rats. Journal of Nuclear Medicine, 2015, 56, 1088-1093.	5.0	24
48	Probabilistic atlas-based segmentation of combined T1-weighted and DUTE MRI for calculation of head attenuation maps in integrated PET/MRI scanners. American Journal of Nuclear Medicine and Molecular Imaging, 2014, 4, 160-71.	1.0	23
49	Proton range shift analysis on brain pseudo-CT generated from T1 and T2 MR. Acta Oncológica, 2018, 57, 1521-1531.	1.8	22
50	On the accuracy and reproducibility of a novel probabilistic atlas-based generation for calculation of head attenuation maps on integrated PET/MR scanners. European Journal of Nuclear Medicine and Molecular Imaging, 2017, 44, 398-407.	6.4	19
51	An Efficient Approach to Perform MR-Assisted PET Data Optimization in Simultaneous PET/MR Neuroimaging Studies. Journal of Nuclear Medicine, 2019, 60, 272-278.	5.0	17
52	DeepStrain: A Deep Learning Workflow for the Automated Characterization of Cardiac Mechanics. Frontiers in Cardiovascular Medicine, 2021, 8, 730316.	2.4	15
53	Detection and Characterization of Thrombosis in Humans Using Fibrin-Targeted Positron Emission Tomography and Magnetic Resonance. JACC: Cardiovascular Imaging, 2022, 15, 504-515.	5.3	12
54	Quantification of receptor–ligand binding potential in sub-striatal domains using probabilistic and template regions of interest. NeuroImage, 2011, 55, 101-112.	4.2	10

#	Article	IF	CITATIONS
55	Intrascanner Reproducibility of an SPM-Based Head MR-Based Attenuation Correction Method. IEEE Transactions on Radiation and Plasma Medical Sciences, 2019, 3, 327-333.	3.7	9
56	Synthesis and evaluation of fluorineâ€18 and copperâ€64 labelled PBR radioligands. Journal of Labelled Compounds and Radiopharmaceuticals, 2007, 50, 561-562.	1.0	7
57	Franken-CT: Head and Neck MR-Based Pseudo-CT Synthesis Using Diverse Anatomical Overlapping MR-CT Scans. Applied Sciences (Switzerland), 2021, 11, 3508.	2.5	7
58	Advanced Multimodal Methods for Cranial Pseudo-CT Generation Validated by IMRT and VMAT Radiation Therapy Plans. International Journal of Radiation Oncology Biology Physics, 2018, 102, 792-800.	0.8	6
59	Masamune: a tool for automatic dynamic PET data processing, image reconstruction and integrated PET/MRI data analysis. EJNMMI Physics, 2014, 1, A57.	2.7	5
60	Evaluation of Deep Learning–Based Approaches to Segment Bowel Air Pockets and Generate Pelvic Attenuation Maps from CAIPIRINHA-Accelerated Dixon MR Images. Journal of Nuclear Medicine, 2022, 63, 468-475.	5.0	5
61	Identifying aortic plaque inflammation as a potential cause of stroke. Journal of Neurology, Neurosurgery and Psychiatry, 2008, 79, 236-236.	1.9	4
62	Reply. Annals of Neurology, 2017, 81, 324-325.	5.3	4
63	Assessment of motion and model bias on the detection of dopamine response to behavioral challenge. Journal of Cerebral Blood Flow and Metabolism, 2022, 42, 1309-1321.	4.3	4
64	New SPM8-based MRAC method for simultaneous PET/MR brain images: comparison with state-of-the-art non-rigid registration methods. EJNMMI Physics, 2014, 1, A29.	2.7	3
65	Combining MRI With PET for Partial Volume Correction Improves Image-Derived Input Functions in Mice. IEEE Transactions on Nuclear Science, 2015, 62, 628-633.	2.0	3
66	Imaging High-Risk Atherothrombosis Using a Novel Fibrin-Binding Positron Emission Tomography Probe. Stroke, 2022, 53, 595-604.	2.0	3
67	Combined MR-assisted motion and partial volume effects corrections – impact on PET data quantification. EJNMMI Physics, 2014, 1, A38.	2.7	2
68	Type I Collagen-Targeted PET Imaging in Idiopathic Pulmonary Fibrosis: First-in-Human Studies. , 2019, , .		1
69	EP-1564: Dosimetric assessment of pseudo-CT based proton planning. Radiotherapy and Oncology, 2017, 123, S842.	0.6	Ο
70	Abstract 324: Molecular Imaging of High Risk Atherosclerotic Plaque Using Fibrin-Binding PET Probe. Arteriosclerosis, Thrombosis, and Vascular Biology, 2018, 38, .	2.4	0
71	Abstract WP526: Molecular Imaging of Carotid Plaques Using a Fibrin-Binding PET Probe. Stroke, 2019, 50, .	2.0	0